 https://doi.org/10.1109/ISSCC42614.2022.9731608

24.2 A 1.66Gb/s and 5.8pJ/b Transcutaneous IR-UWB Telemetry System with Hybrid Impulse Modulation for Intracortical Brain-Computer Interfaces

Minyoung Song[1], Yu Huang[1,2], Yiyu Shen[1], Chengyao Shi[1,3], Arjan Breeschoten[1], Mario Konijnenburg[1], Huib Visser[1], Jac Romme[1], Barundeb Dutta[4], Morteza S. Alavi[2], Christian Bachmann[1], Yao-Hong Liu[1]

[1]imec-Netherlands, Eindhoven, The Netherlands, [2]Delft University of Technology, Delft, The Netherlands, [3]Eindhoven University of Technology, Eindhoven, The Netherlands, [4]imec, Leuven, Belgium

Intra-cortical extracellular neural sensing is being rapidly and widely applied in several clinical research and brain-computer interfaces (BCIs), as the number of sensing channels continues to double every 6 years. By distributing multiple high-density extracellular micro-electrode arrays (MEAs) *in vivo* across the brain, each with 1000's of sensing channels, neuroscientists have begun to map the correlation of neuronal activity across different brain regions, with the single-neuron precision [1]. Since each neural sensing channel typically samples at 20-50kSps with a >10b ADC, multiple MEAs demand a data transfer rate up to Gbps. However, these BCIs are severely hindered in many clinical uses due to the lack of a high-data-rate and miniature wireless telemetry solution that can be implanted below the scalp, i.e., transcutaneously (Fig. 24.2.1). The area of the wireless telemetry module should be miniaturized to ~3cm^2 due to neurosurgical implantation constraints. The transmission range up to 10cm is highly desirable, in order to improve the reliability of the wireless link against e.g., antenna misalignment, etc. Finally, the power consumption of the wireless telemetry should be limited to ~10mW to minimize thermal flux from the module's surface area, avoiding excessive tissue heating. Most of the conventional transcutaneous wireless telemetry adopt inductive coupling, but the data rate is limited to a few Mbps. A near-infrared (NIR) optical transcutaneous TX using a vertical cavity surface emitting laser (VCSEL) [2] demonstrated a data rate up to 300Mbps but suffers from a limited transmission range (4mm) and requires a sub-mm precise alignment between the implant TX and a wearable RX. Impulse-radio UWB (IR-UWB) is promising for the targeted requirements [3-5].

This paper presents a transcutaneous IR-UWB TX with a record high data rate, while achieving up to 10× longer transmission range and with performance well within the volumetric and heat dissipation constraints. Three innovations are introduced: 1) a hybrid impulse modulation combining M-PPM, M-PSK and M-PAM for maximizing the link budget, 2) a power-efficient delay generator for a calibration-free M-PPM, 3) a low-noise 8-phase ring oscillator (RO) with duty-cycle correction for an accurate M-PSK. The state-of-the-art IR-UWB TX achieves 1.125Gbps data rate by adopting digitalized multi-pulse-position-modulation (D-MPPM) with a fine time step of ~50ps [3]. However, based on Euclidean distance, high Eb/N0 is required to discriminate between two adjacent pulse positions as the modulation order increases. This is not feasible in the targeted scenarios where the miniature antenna and tissue at UWB frequency can introduce up to 60dB of path loss. In this work, we propose a 3-D hybrid impulse modulation (4PAM-8PSK-4PAM) that employs an agile digital polar-based IR-UWB TX. This approach achieves high data rate with the modulation order of 7, while significantly reducing the Eb/N0 requirement by ~20dB compared to M-PPM (Fig. 24.2.2). One key challenge of the proposed approach is to ensure a high level of independence among different modulations with low power overhead when performed simultaneously. Prior IR-UWB TXs perform impulse modulation with either carrier-less [3][4] or up-conversion approaches [5]. The carrier-less TXs use edge-combining which leverage the fast-switching digital logic in nanoscale CMOS, thus power-efficient and requiring no dedicated LO. However, simultaneously performing M-PPM and M-PSK in carrier-less TXs is challenging, since both phase and time need to be modulated via delay edges. The classical IQ-based up-conversion method can perform the high order modulation, but limit to achieving high energy efficiency. The polar-based up-conversion TX [5] consumes low power, as the pulse shaping is performed asynchronously with delay cells and digitally-controlled PA (DPA). However, it is limited to support only BPSK.

Figure 24.2.1 shows the proposed low power polar-based IR-UWB TX capable of the hybrid impulse modulation. The impulse waveform is shaped by the DPA and a pulse shaper (PS) which uses delay cells to perform FIR filtering in RF domain. An injection-locked RO (ILRO) is adopted to provide low jitter, 8 phases for 8PSK in a wide frequency range. A 7b 238MSym/s digital data is distributed to three different modulation paths, PAM, PSK, and PPM, after being synchronized with a 476MHz system clock (SYS_CLK). The switch-cap DPA with 32-unit cells supports up to 4PAM. The 8PSK is performed by selecting one of 8 phases from the ILRO using a phase selector (PHMUX). By accurately delaying the impulse with a PPM control (PPM_CTRL), precise 4PPM can be supported.

Figure 24.2.2 illustrates the timing diagram of the proposed 3-D hybrid impulse modulation. To avoid "inter-modulation" between PPM and PSK, the carrier phase is set at the beginning of each impulse symbol. To trigger an impulse, a 25% duty-cycled unit pulse (UNIT_PUL) at 238MHz is generated from the SYS_CLK. The PPM_CTRL shown in Fig. 24.2.2 modulates the delay of the UNIT_PUL according to the PPM data, and its output (PPM_OUT) is then fed to the PS to synthesize a triangular-shaped impulse. The pulse width of the impulse (T_{PULSE}) is set to ~2ns by the PS, and the symbol period (T_{SYMBOL}) is set by two cycles of the SYS_CLK to be 4.2ns. This ensures a sufficient time range (T_{PPM}) to perform 4PPM and avoids potential impact from inter-symbol interference or multi-path. The PPM time step (T_{PPM_STEP}) of 600ps is chosen according to the targeted Eb/N0 requirement (Fig. 24.2.2) and the PPM control complexity. The delay step is the quadruple of DCO_OUT (T_{DCO}). As long as the DCO is injection locked by the SYS_CLK, no extra delay calibration is required. The proposed PPM_CTRL only dissipates 115µW.

The proposed DCO is shown in Fig. 24.2.3. To reduce the antenna dimension and minimize harmonic pulling from the inductive powering [4], the DCO frequency is targeted to 6 to 9GHz, i.e., the high band of UWB. Generating 8 phases with a RO at up to 9GHz is challenging because it requires multiple delay stages for 8PSK. A negative skewing technique [6][7] is adopted for reducing the delay of each stage. In each delay cell, its PMOS (IPP/IPN) input is forwarded to the NMOS (INP/INN) one stage ahead, resulting in a faster transition and lower phase noise. However, this approach increases the duty cycle error, which degrades the 8PSK accuracy. The proposed DCO buffer with a feedback duty cycle correction is embedded in each delay cell with low capacitive loading and recovers the amplitude disturbance due to injection-locking, critical to ensure M-PAM accuracy. It can correct the duty cycle error within 5ns, and each consumes only 120µW. The measured phase error of the proposed DCO is 2.6° at 6.7GHz, sufficient for low EVM (<-20dB) for 8PSK modulation.

The proposed UWB TX IC was fabricated in 28nm CMOS, occupying only 0.155mm^2, including an on-chip antenna matching network. The wireless module implemented on an FR4 PCB has a core electronic area of only 1.05cm^2, including a printed circular monopole antenna sized 9.4×7mm^2 and the TX IC (Fig. 24.2.7). The simulated antenna gain is -6 to -9dBi based on a human head model. An impulse modulation in time domain, an "eye-diagram" of the impulse envelope and a constellation in complex plane of the hybrid modulation are shown in Fig. 24.2.4 demonstrate a high modulation quality. The DPA has a measured peak output power of 0dBm, and the measured DPA output spectrum complies to the FCC mask (Fig. 24.2.5), even without the attenuation of the tissue. To test the transmission range, the wireless module is inserted in a 15mm-thickness, multi-layer porcine tissue, placed at various distances away from an UWB RX composed of a 15cm^2 5dBi antenna, a 3dB-NF LNA and a high-speed oscilloscope as an ADC. The measured transmission ranges are 2 and 15cm at 1.66 and 1.43Gbps data rates, respectively, for bit-error rate (BER) below 10^{-4}. Figure 24.2.6 summarizes the performance and benchmarks with state-ot-the-art transcutaneous and high data rate UWB TXs. The presented IR-UWB TX achieves the highest data rate with longest range under the implant condition, leading to the best-in-class range normalized energy-efficiency of 45pJ/bit/m.

Acknowledgement:
This project has received funding from the European Research Council (ERC) under the European Union's Horizon 2020 research and innovation programme (grant agreement No. 101001448).

References:
[1] C. Stringer, et al., "Spontaneous Bahaviors Drive Multidimensional, Brain-Wide Activity, " in *Science*, vol. 36, no. 6437, April 2019.
[2] A. D. Marcellis et al., "A 300 Mbps 37 pJ/bit Pulsed Optical Biotelemetry," in *IEEE TBioCAS*, vol.14, no.3, pp. 441-451, Jun. 2020.
[3] G. Lee, et al., " A 1.125Gb/s 28mW 2m-Radio-Range IR-UWB CMOS Transceiver," *ISSCC*, pp. 302-303, Feb. 2021.
[4] S. Mirbozorgi, et al., " A Single-Chip Full-Duplex High Speed Transceiver for Multi-Site Stimulating and Recording Neural Implants" in *IEEE TBioCAS*, vol.10, no.3, pp. 643-653, Jun. 2016.

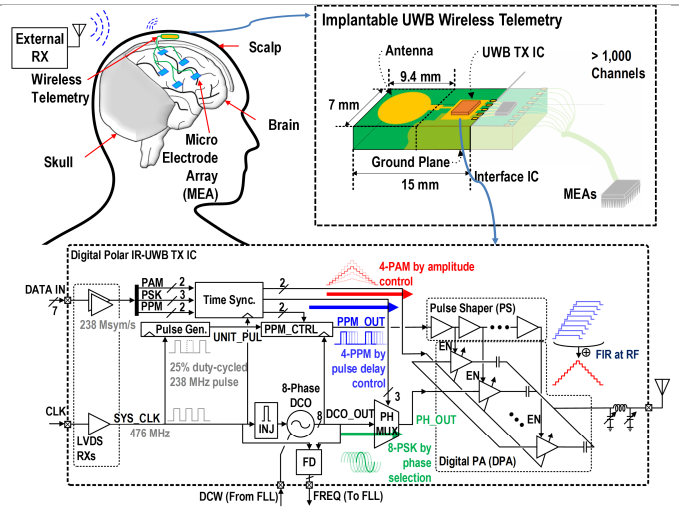

Figure 24.2.1: Conceptual diagram of intra-cortical neural sensing with 1.05cm² implantable UWB wireless telemetry (top) and block diagram of proposed UWB transmitter (TX).

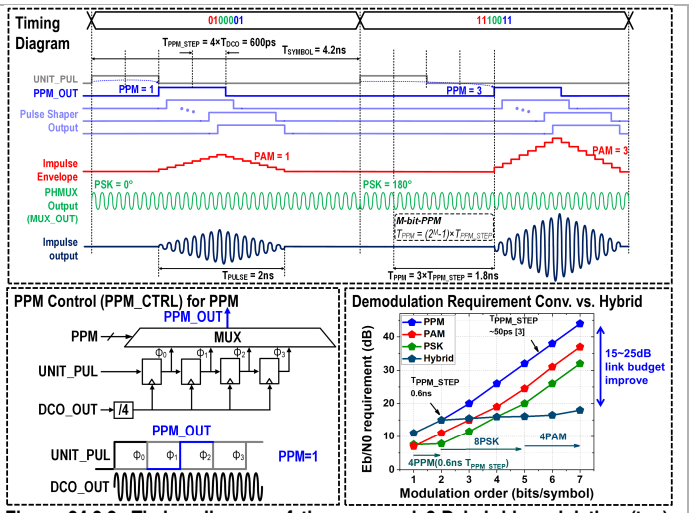

Figure 24.2.2: Timing diagram of the proposed 3-D hybrid modulation (top), proposed calibration-free PPM control circuit (bottom-left), and demodulation requirements for conventional modulations and proposed 3-D hybrid modulation (bottom-right).

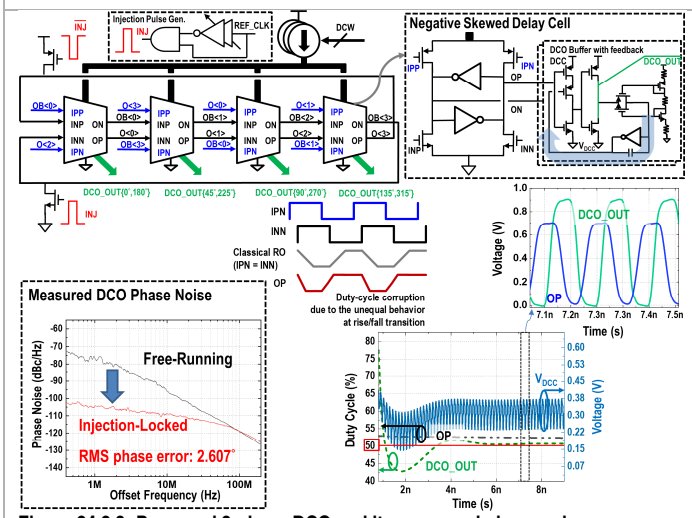

Figure 24.2.3: Proposed 8-phase DCO and its measured phase noise.

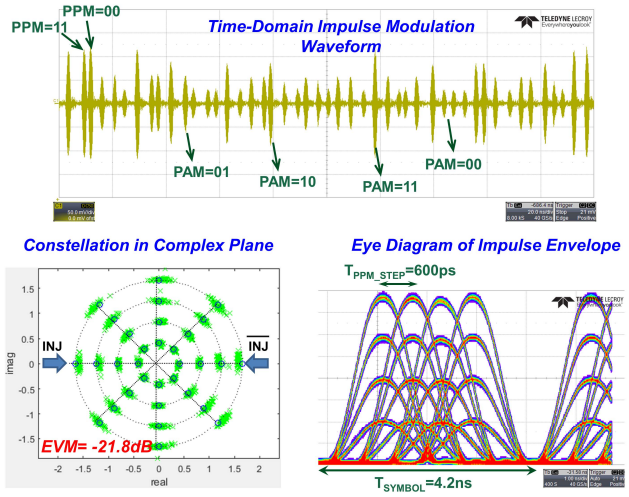

Figure 24.2.4: Measured time-domain impulse modulation waveform (top), constellation in complex plain (bottom-left), and envelope eye diagram of the proposed hybrid impulse modulation.

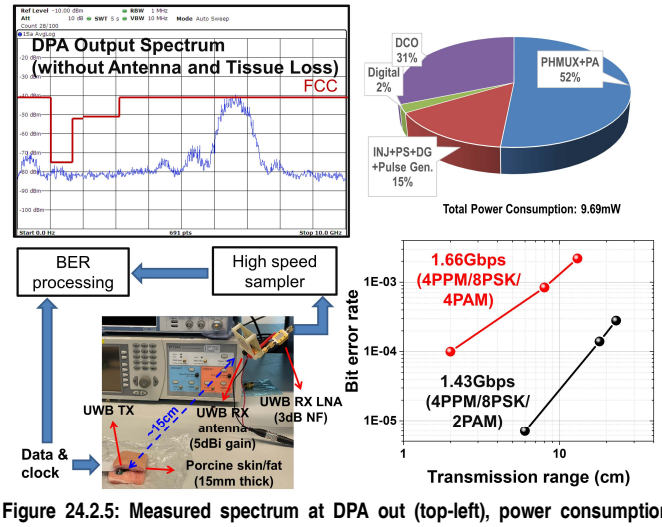

Figure 24.2.5: Measured spectrum at DPA out (top-left), power consumption (top-right), *in vitro* wireless measurement setup (bottom-left), and measured BER of 1.43 Gbps and 1.66 Gbps data rates at various transmission ranges.

	This work	[4]	Ando, TBioCAS'16	[2]	[3]	[5]
Device technology	28nm CMOS	180nm CMOS	GaAs HBT	VCSEL	65nm CMOS	28nm CMOS
Wireless method	IR-UWB	IR-UWB	IR-UWB	Optical	IR-UWB	IR-UWB
Frequency	6-9GHz	3-7GHz	8GHz	NIR	4GHz	3-10GHz
Modulation	4PPM+8PSK+ 4PAM impulse	BPSK impulse	OOK impulse	OOK impulse	D-MPPM impulse	BPSK impulse
TX architecture	Digital polar (DPA+ PHMUX)	Edge combine	Edge combine	-	Edge combine	Digital polar (DPA+ ILRO)
Max. data rate	**1.66Gbps**	500Mbps	128Mbps	300Mbps	1.125Gbps	27Mbps
TX power cons.	9.69mW	5.4mW	561mW	11mW	28mW	4.9mW
TX energy efficiency.	**5.8pJ/b**	10.8pJ/b	438pJ/b	37pJ/b	25pJ/b	180pJ/b
TX peak P_{OUT}	0dBm	N.A.	-12.3dBm	-	-10dBm	-0.7dBm
TX antenna area	66mm²	100mm²	N.A.	N.A.	N.A.	-
TX antenna gain	-8.5dBi	N.A.	N.A.	-	3dBi	-
Tissue thickness	15mm skin/fat	2mm skin/fat & 4mm bone	15-20mm phantom	3.5mm skin	No tissue	No tissue
Transmission range (in-vitro)	**2cm**@1.66Gbps **15cm**@1.43Gbps	1.5cm	1cm	0.4cm	N.A.**	-**
Normalized energy effi.*	**45pJ/b/m** (@1.43Gbps)	720pJ/b/m	43.8nJ/b/m	9.25nJ/b/m	-	-

*TX energy efficiency normalized to 1m transmission range. ** No transmission range reported with tissue or phantom.

Figure 24.2.6: Performance summary and comparison table with prior arts.

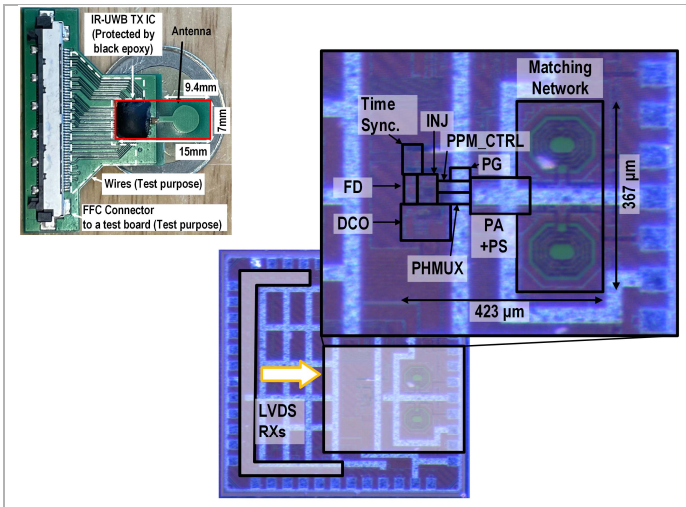

Figure 24.2.7: Die micrograph and prototype of the wireless module.

Additional References:
[5] E. Allebes et al., "A 3-to-10GHz 180pJ/b IEEE802.15.4z/4a IR-UWB Coherent Polar Transmitter in 28nm CMOS with Asynchronous Amplitude Pulse-Shaping and Injection-Locked Phase Modulation," *ISSCC*, pp. 304-305, Feb. 2021. [6] S. -J. Lee et al., "A Novel High-Speed Ring Oscillator for Multiphase Clock Generation Using Negative Skewed Delay Scheme," in *IEEE JSSC*, vol. 32, no. 2, pp. 289-291, Feb. 1997. [7] M. Song, et al., "A 2.4 GHz 0.1-Fref-Bandwidth All-Digital Phase-Locked Loop With Delay-Cell-Less TDC," in *IEEE TCAS-I*, vol.60, no.12, pp. 3145-3151, Dec. 2013.